Backbone Dynamics of Proteins As Studied by ^{15}N Inverse Detected Heteronuclear NMR Spectroscopy: Application to Staphylococcal Nuclease†

Lewis E. Kay,‡ Dennis A. Torchia,§ and Ad Bax*,‡

Laboratory of Chemical Physics, National Institute of Diabetes and Digestive and Kidney Diseases, and Bone Research Branch, National Institute of Dental Research, National Institutes of Health, Bethesda, Maryland 20892

Received July 13, 1989; Revised Manuscript Received September 7, 1989

ABSTRACT: This paper describes the use of novel two-dimensional nuclear magnetic resonance (NMR) pulse sequences to provide insight into protein dynamics. The sequences developed permit the measurement of the relaxation properties of individual nuclei in macromolecules, thereby providing a powerful experimental approach to the study of local protein mobility. For isotopically labeled macromolecules, the sequences enable measurements of heteronuclear nuclear Overhauser effects (NOE) and spin–lattice (T_1) and spin–spin (T_2) ^{15}N or ^{13}C relaxation times with a sensitivity similar to those of many homonuclear ^1H experiments. Because T_1 values and heteronuclear NOEs are sensitive to high-frequency motions (10^8–10^{12} s^{-1}) while T_2 values are also a function of much slower processes, it is possible to explore dynamic events occurring over a large time scale. We have applied these techniques to investigate the backbone dynamics of the protein staphylococcal nuclease (S. Nase) complexed with thymidine 3′,5′-bisphosphate (pdTp) and Ca^{2+} and labeled uniformly with ^{15}N. T_1, T_2, and NOE values were obtained for over 100 assigned backbone amide nitrogens in the protein. Values of the order parameter (S), characterizing the extent of rapid ^1H–^{15}N bond motions, have been determined. These results suggest that there is no correlation between these rapid small amplitude motions and secondary structure for S. Nase. In contrast, ^{15}N line widths suggest a possible correlation between secondary structure and motions on the millisecond time scale. In particular, the loop region between residues 42 and 56 appears to be considerably more flexible on this slow time scale than the rest of the protein.

NMR[1] relaxation studies can provide detailed information pertaining to the internal dynamics occurring in proteins. Interest in measuring relaxation parameters has, in part, stemmed from molecular dynamics studies of several protein systems (Levy et al., 1981; Olejniczak et al., 1984; Brünger et al., 1987; LeMaster et al., 1988). These investigations have shown that, despite the close packing in globular proteins, there are substantial fluctuations on the picosecond time scale. Moreover, differences in cross-peak intensities in two-dimensional homonuclear and heteronuclear NMR experiments suggest that in proteins there is a wide range of low-frequency motions (millisecond time scale). In addition to providing a more complete description of the system studied than is available from a static structure, knowledge of motional properties may be important for understanding functional aspects (Brünger et al., 1987).

The measurement of ^{15}N or ^{13}C relaxation rates is particularly useful for obtaining dynamic information since the relaxation of these nuclei is governed predominantly by the dipolar interaction with directly bound protons and to a much smaller extent by the chemical shift anisotropy mechanism (Allerhand et al., 1971a). These interactions have been well characterized by studies on model systems (Kuhlmann et al., 1970; Hiyama et al., 1988) and can be interpreted in terms of dynamic molecular properties without a detailed understanding of the structural properties of the system in question. The utility of ^{13}C and ^{15}N relaxation studies for obtaining dynamic properties of macromolecules was recognized early on by Allerhand and co-workers (Allerhand et al., 1971b; Glushko et al., 1972), who measured ^{13}C spin–lattice relaxation times of carbonyl and aliphatic carbons at natural abundance in ribonuclease, by Roberts and co-workers (Gust et al., 1975), who measured ^{15}N T_1s and nuclear Overhauser enhancements (NOEs) at natural abundance for several biopolymers, and by Hawkes and co-workers (Hawkes et al., 1975), who reported on a natural abundance ^{13}C and ^{15}N NMR relaxation study of the cyclic decapeptide gramacidin S. Since the mid-1970s a large number of papers have appeared dealing with the extraction of dynamic molecular properties from ^{13}C or ^{15}N relaxation studies (Norton et al., 1977; Llinas et al., 1978; London, 1980; Richarz et al., 1980; Fuson et al., 1983; Henry et al., 1986; McCain et al., 1986, 1988; Smith et al., 1987; Bogusky et al., 1987; Schiksnis et al., 1989; Dellwo & Wand, 1989). These studies have involved direct observation of $^{13}C/^{15}N$, using one-dimensional NMR techniques. Unfortunately, the low sensitivity of these heteronuclei leads to the requirement of large amounts of sample and long measuring times, while the lack of resolution in one-dimensional NMR spectra limits the measurements to the extraction of bulk relaxation times or relaxation values of only a small number of selectively labeled spins. These problems can be largely circumvented by using one- and two-dimensional pulse schemes that enable indirect measurement of the relaxation properties of insensitive nuclei (Kay et al., 1987; Sklenář et al., 1987; Nirmala & Wagner, 1988, 1989).

† This work was supported by the Intramural AIDS Antiviral Program of the Office of the Director of the National Institutes of Health. L.E.K. acknowledges financial support from the Medical Research Council of Canada and the Alberta Heritage Trust Foundation.

‡ Laboratory of Chemical Physics, National Institute of Diabetes and Digestive and Kidney Diseases.

§ Bone Research Branch, National Institute of Dental Research.

[1] Abbreviations: CPMG, Carr–Purcell–Meiboom–Gill; CSA, chemical shift anisotropy; γ, gyromagnetic ratio; HMQC, heteronuclear multiple quantum correlation; NOE, nuclear Overhauser enhancement; NMR, nuclear magnetic resonance; pdTp, thymidine 3′,5′-bisphosphate; S, order parameter; S. Nase, staphylococcal nuclease; T_1, spin–lattice relaxation time; T_2, spin–spin relaxation time; τ_m, overall molecular correlation time; τ_e, effective correlation time describing rapid internal motions; TPPI, time proportional phase incrementation.

0006-2960/89/0428-8972$01.50/0

In this paper we present a ^{15}N NMR relaxation study of the backbone dynamics of the protein staphylococcal nuclease (S. Nase) complexed with thymidine 3',5'-bisphosphate (pdTp) and Ca^{2+}, having a total molecular mass of 18 kDa. Because nearly complete assignment of the ^{15}N backbone atoms has been obtained for S. Nase, it provides an ideal target for investigating local motional dynamics by ^{15}N NMR.

Methods

Protein Purification and ^{15}N Labeling. The uniformly ^{15}N-enriched nuclease sample was obtained from transformed *Escherichia coli* containing an expression plasmid, pNJS, that encoded for the production of the wild-type (149 residues) enzyme. The cell growth conditions and protein purification procedures have been described previously (Hibler et al., 1987; Torchia et al., 1989).

NMR Spectroscopy. Schemes a and b of Figure 1 show the pulse sequences used to record ^1H–^{15}N correlation spectra for measuring ^{15}N T_1 and T_2 relaxation rates. The experiments are variations of a sequence originally proposed for the recording of ^1H–^{15}N correlation spectra (Bodenhausen & Ruben, 1980). In order to measure T_1 or T_2 relaxation rates of the heterospin, net magnetization transfer between the proton(s) and the coupled heteroatom must occur, requiring slightly more complicated pulse sequences than necessary for a normal single quantum heteronuclear correlation experiment. Two refocused INEPT-type sequences (Morris & Freeman, 1979; Burum & Ernst, 1980) are employed to transfer magnetization from the directly bound protons to the low γ heteronucleus and back to protons for detection. In this way the detected signal intensity is independent of the gyromagnetic ratio (γ) of the heteroatom, providing an approximately 30-fold increase in sensitivity relative to ^1H–^{15}N correlations recorded with ^{15}N detection (Bax et al., 1989a). T_1 or T_2 values are extracted in a straightforward fashion by measuring the intensities of cross-peaks in 2D maps as a function of a relaxation delay, T.

Figure 1c illustrates the new pulse sequence developed to record correlation spectra for measuring ^1H–^{15}N NOEs. Spectra are recorded in the presence and absence of ^1H saturation. Since the longitudinal magnetization of the heteroatom is to be measured for calculating the heteronuclear NOE, magnetization must originate on the ^{15}N spin. Magnetization is subsequently transferred via a refocused INEPT sequence to the directly coupled NH proton for observation.

All spectra were recorded with a sample of 1.5 mM S. Nase in 90% H_2O–10% D_2O complexed pdTp (5 mM) and Ca^{2+} (10 mM) at pH 6.4 and at a temperature of 35 °C. T_1 spectra were recorded at 270 MHz on a NT270 spectrometer, at 500 MHz on a Bruker AM500 spectrometer, and at 600 MHz on a Bruker AM600 spectrometer. T_2 and NOE data sets were recorded at 500 MHz on a Bruker AM500 spectrometer.

In order to obtain quadrature in F_1, data were recorded at 270 MHz according to the method of States et al. (1982). Two-dimensional spectra consisting of 128 complex t_1 points and 256 complex t_2 points were acquired with 256 scans per t_1 point. To obtain T_1 relaxation rates, four T delays of 55, 122, 190, and 245 ms were employed. On the Bruker spectrometers, F_1 quadrature was achieved with TPPI (Marion & Wüthrich, 1983). A 512 × 1024 real data matrix was acquired for each duration T, with 32 scans per t_1 increment. T_1 values were obtained by using six T delays of 50, 190, 330, 470, 610, and 750 ms at 500 MHz and 50, 210, 370, 530, 690, and 850 ms at 600 MHz. T_2 values were recorded at 500 MHz by using six delay values: 4.8, 24.0, 43.2, 62.4, 86.4, and 105.6 ms. NOE data sets were recorded as 512 × 1024 real matrices with TPPI to achieve quadrature in F_1 with 72 scans per t_1 point for the spectrum recorded with the NOE and 32 scans per t_1 point for the spectrum recorded without the NOE. The T_1, T_2, and NOE data sets were processed with

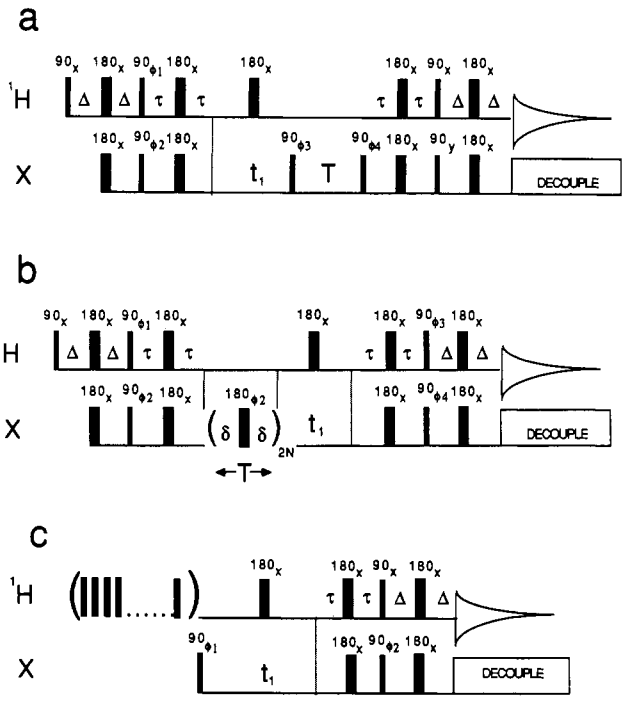

FIGURE 1: Schemes for the measurements of X spin T_1 (a), T_2 (b), and ^1H–X NOE values (c) with ^1H detection. For the case where spectra are recorded in H_2O (i.e., where X = ^{15}N), effective water suppression is achieved with the use of an off-resonance DANTE sequence described previously (Kay et al., 1989). The value of Δ is slightly less than $1/(4J_{XH})$ (2.3 ms for ^{15}N) to minimize relaxation losses. Because the transverse relaxation times for backbone ^{15}N spins are long, the value of τ is set to $1/(4J_{XH})$ (2.75 ms). For spectra recorded in H_2O, water saturation during the relaxation period T is achieved by the use of DANTE pulses. The phase cycling employed for (a) is $\phi_1 = 8(y), 8(-y)$, $\phi_2 = 4(x), 4(-x)$, $\phi_3 = -y, y$, and $\phi_4 = 2(x), 2(-x)$; Acq = $x, -x, -x, x, -x, x, x, -x$. The receiver phase is inverted every eight scans. A composite 180° pulse ($90_x180_y90_x$) is applied in the center of the t_1 evolution period. The effect of the phase alternation of ϕ_3 is to alternately store magnetization along the $+Z$ axis and $-Z$ axis so that magnetization relaxes as $\exp(-T/T_1)$. In this way a nonoptimal delay between scans will only affect the sensitivity of the experiment without introducing systematic errors (Sklenář et al., 1987). Quadrature in F_1 is achieved by incrementing the phase of ϕ_3 by 90° for each successive t_1 point, time proportional phase incrementation (TPPI) (Marion & Wüthrich, 1983). For sequence b, τ must be set to $1/(4J_{XH})$ (~2.75 ms for ^{15}N) so that all X magnetization is in phase at the start of the CPMG portion of the sequence. For T_2 spectra recorded in water, application of a 180° ^1H pulse in the middle of the relaxation period (i.e., at $T/2$) inverts the water magnetization so that at the end of the relaxation delay, T, very little net water recovery along the Z axis has occurred. The phase cycle employed for (b) is $\phi_1 = y, -y$, $\phi_2 = 2(x), 2(-x)$, $\phi_3 = 4(x), 4(-x)$, and $\phi_4 = 8(x), 8(-x)$; Acq = $x, -x, -x, x, 2(-x, x, x, -x), x, -x, -x, x$. After 16 scans, the phase of the first 180° pulse on X after the evolution period, t_1, is inverted without changing the receiver phase. This pulse and the pulse at the center of the evolution period are composite 180° pulses. Quadrature in F_1 is achieved via a TPPI of ϕ_4. In order to measure ^1H–^{15}N NOEs, data sets with and without ^1H saturation are recorded. Scheme c indicates the sequence used for the case of ^1H saturation. ^1H saturation is achieved by the application of 120° pulses spaced at 20-ms intervals for 3 s prior to the first ^{15}N pulse [not to scale in (c)] (Markley et al., 1971). Water suppression is achieved with the use of an off-resonance DANTE sequence (Kay et al., 1989) during this time period. For the data set recorded without the NOE, water suppression is achieved in a very short period of approximately 100 ms in order to minimize spin diffusion to the rest of the protein. The phase cycle employed for (c) is $\phi_1 = x, -x$ and $\phi_2 = y, y, -y, -y$; Acq = $x, -x, -x, x$. Quadrature in F_1 is achieved by a TPPI of ϕ_1.

software provided by New Methods Research (Syracuse, NY). Intensities of cross-peaks were obtained from peak-picking routines provided in the software package.

Analysis of T_1 and T_2 Relaxation Times and NOE Enhancements. The T_1 and T_2 relaxation rates and the NOE enhancement of an amide ^{15}N spin relaxed by dipolar coupling to a directly bonded proton and by chemical shift anisotropy are given by (Abragam, 1961)

$$1/T_1 = d^2\{J(\omega_A - \omega_X) + 3J(\omega_X) + 6J(\omega_A + \omega_X)\} + c^2J(\omega_X) \quad (1)$$

$$1/T_2 = 0.5d^2\{4J(0) + J(\omega_A - \omega_X) + 3J(\omega_X) + 6J(\omega_A) + 6J(\omega_A + \omega_X)\} + \tfrac{1}{6}c^2\{3J(\omega_X) + 4J(0)\} \quad (2)$$

and

$$\mathrm{NOE} = 1 + [(\gamma_A/\gamma_X)d^2\{6J(\omega_A + \omega_X) - J(\omega_A - \omega_X)\}T_1] \quad (3)$$

with $d^2 = 0.1\gamma_A^2\gamma_X^2h^2/(4\pi^2)\langle 1/r_{AX}^3\rangle^2$ and $c^2 = (2/15)\gamma_X^2H_0^2(\sigma_\parallel - \sigma_\perp)^2$. In eq. 1–3 A = ^1H, X = ^{15}N, γ_i is the gyromagnetic ratio of spin i, h is Planck's constant, r_{AX} is the internuclear ^1H–^{15}N distance, H_0 is the magnetic field strength, $\sigma_\parallel$ and $\sigma_\perp$ are the parallel and perpendicular components of the axially symmetric ^{15}N chemical shift tensor, and $J(\omega_i)$ is the spectral density function. The assumption of an axially symmetric chemical shift tensor has been shown to be valid for peptide bonds, with $\sigma_\parallel - \sigma_\perp = -160$ ppm (Hiyama et al., 1988).

For a protein in solution $J(\omega_i)$ depends on both the overall motion of the macromolecule as a whole and on the internal motions of the ^1H–^{15}N bond vector. The analysis of the relaxation data in terms of the minimum number of unique motional parameters is most easily achieved by using the formalism of Lipari and Szabo (1982a,b). These authors express $J(\omega_i)$ according to

$$J(\omega_i) = S^2\tau_m/[1 + (\omega_i\tau_m)^2] + (1 - S^2)\tau/[1 + (\omega_i\tau)^2] \quad (4)$$

where S is an order parameter measuring the degree of spatial restriction of the motion, τ_m is the correlation time for the overall motion, and $1/\tau = 1/\tau_m + 1/\tau_e$, where τ_e is an effective correlation time describing the rapid internal motions. Implicit in this model is that the overall tumbling of the macromolecule is isotropic. As will be discussed later, this is a reasonable assumption for S. Nase. The parameters S and τ_e described above are defined in a model-independent way but can be easily interpreted within the framework of some physically reasonable model (Lipari & Szabo, 1982a,b; Brainard & Szabo, 1981).

In order to gain physical insight into the effects of τ_m, τ_e, and S^2 on the measurables T_1, T_2, and NOE, it is convenient to recast eq 1–3 to

$$1/T_1 = S^2(1/T_1)_{isot}[1 + (10 + \delta)/(3 + \delta) \times \{(1 - S^2)/S^2\}(\tau_e/\tau_m)(\omega_X\tau_m)^2] \quad (5)$$

$$1/T_2 = S^2(1/T_2)_{isot}[1 + \{10 + (7/6)\delta\}/\{2 + (2/3)\delta\} \times \{(1 - S^2)/S^2\}(\tau_e/\tau_m)] \quad (6)$$

$$\mathrm{NOE} = \mathrm{NOE}_{isot} - 50/(3 + \delta)[\{(1 - S^2)/S^2\}(\tau_e/\tau_m)(\omega_X\tau_m)^2] \quad (7)$$

where the subscript isot refers to the value in the absence of internal motions and $\delta = (c/d)^2$. The value of δ is 0.67 for a ^{15}N resonance frequency of 50.7 MHz. This corresponds to a contribution to the ^{15}N spin–lattice relaxation of 82% and 18% from the ^1H–^{15}N dipolar and CSA relaxation mechanisms, respectively. Equations 5–7 have been derived with the assumptions that $\{(\omega_A \pm \omega_X)\tau_e\}^2 \ll 1$, $(\omega_X\tau_m)^2 \gg 1$, and $\{(\omega_A \pm \omega_X)\tau_m\}^2 \gg (\omega_X\tau_m)^2$. It is readily seen that the NOE is approximately 5 and 30 times more sensitive to internal dynamics than $1/T_1$ and $1/T_2$, respectively, for molecules the size of S. Nase with $\omega_X\tau_m \sim 3$. For example, for $S^2 = 0.9$ and $\tau_m = 9.0$ ns, the value of the NOE varies from 0.80 to 0.66 as τ_e is increased from 0.0 to 0.1 ns. In contrast, $1/T_1$ changes by only 3% over the same range of τ_e values.

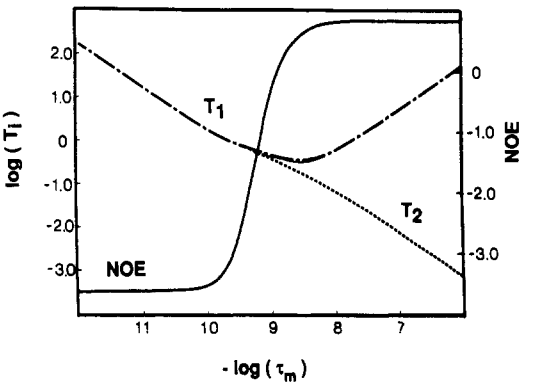

FIGURE 2: Plots of log (T_i|i = 1,2}) and ^1H–^{15}N NOE vs log (τ_m) for ^{15}N relaxed by ^1H–^{15}N dipolar and CSA interactions at a nitrogen frequency of 50.7 MHz. An N–H bond vector tumbling isotropically with $S^2 = 1.0$ and a bond length of 1.02 Å was assumed. A value of $\sigma_\parallel - \sigma_\perp = -160$ ppm was used.

Figure 2 shows plots of the ^{15}N T_1 and T_2 relaxation rates and the ^1H–^{15}N NOE at a ^{15}N frequency of 50.7 MHz as a function of correlation time, τ_m, assuming isotropic overall motion and the absence of internal motions. We have included the effects of ^1H–^{15}N dipolar interactions as well as contributions from chemical shift anisotropy. The NOE can very from −3.6 for $\omega_X\tau_m \ll 1$ to +0.82 for $\omega_X\tau_m \gg 1$. If the dipolar interaction is considered exclusively, the NOE varies from −3.9 to +0.78. In this context, we indicate that in the calculation of relaxation properties for coupled spins of oppositely signed magnetic moments both the sign of the gyromagnetic ratio and the sense of the angular precession of the spins must be taken into account (Werbelow, 1987). This implies that, for a ^{15}N–^1H pair, $(\omega_A + \omega_X) < (\omega_A - \omega_X)$ and $J(\omega_A + \omega_X) > J(\omega_A - \omega_X)$. The literature value of 0.88 for the ratio of ^{15}N signal intensities in the presence and absence of proton saturation in the slow limit (Gust et al., 1975; Hawkes et al., 1975) is incorrect since the opposite sense of precession of the ^1H and ^{15}N spins has been ignored.

For the case of ^{15}N relaxation, the spectral density function described by eq 4 can be simplified considerably. An average NOE value of 0.77 with a standard deviation of 0.07 was obtained on the basis of measuring ^{15}N intensities in the presence and absence of proton saturation for 101 residues in S. Nase. Residues showing negative intensities in the presence of ^1H saturation were excluded before averaging. In addition, Leu-7 and His-8 were also excluded from the average since the NOE values associated with these residues are also significantly decreased by internal motion. As mentioned above, for rigid proteins tumbling isotropically the maximum NOE possible is +0.82. On the basis of an average measured NOE of 0.77, the internal motions contribute, therefore, no more than 6% to the measured NOE for S. Nase. Equations 5 and 7 indicate that neglect of the effects of the second term in eq 4 in this case will contribute no more than a 1% error to $1/T_1$, on average. Even for the few cases where the measured NOE value is one standard deviation below the average, the contribution to $1/T_1$ due to this term is only ~2%. We have, therefore, neglected the effects of τ_e in the interpretation of the T_1 and T_2 data in terms of motional parameters for all residues except those for which a small positive or a negative NOE indicates that such a simplification is not warranted.

This situation is to be contrasted with the case of ^{13}C relaxation, where rapid internal motion can make a measurable contribution to the spin–lattice relaxation rate. For example, increases in ^{15}N longitudinal relaxation rates by 3% due to rapid internal motions translate into increases of about 20% for ^{13}C spin–lattice relaxation rates, assuming identical motional parameters in both cases.

Since, for S. Nase, the expressions for the ^{15}N T_1 and T_2 relaxation rates are essentially independent of τ_e, the overall correlation time τ_m can be extracted on a residue by residue basis according to the expression

$$T_1/T_2 \sim [d^2\{J'(\omega_A - \omega_X) + 3J'(\omega_X) + 6J'(\omega_A + \omega_X)\} + c^2J'(\omega_X)]/[0.5d^2\{4J'(0) + J'(\omega_A - \omega_X) + 3J'(\omega_X) + 6J'(\omega_A) + 6J'(\omega_A + \omega_X)\} + \tfrac{1}{6}c^2\{3J'(\omega_X) + 4J'(0)\}] \quad (8)$$

where T_1 and T_2 are the measured T_1 and T_2 relaxation rates for each ^{15}N spin. In eq 8, $J'(\omega_i)$ is a simplified spectral density function of the form:

$$J'(\omega_i) = S^2\tau_m/[1 + (\omega_i\tau_m)^2] \quad (9)$$

Equation 8 is independent of S^2, and τ_m is readily obtained by a computer minimization of the difference between the left- and right-hand sides of eq 8 for each T_1/T_2 ratio. The value for S^2 at each ^{15}N site can then be obtained from either eq 1 or eq 2 by using an average value of τ_m.

Results and Discussion

In the interpretation of the relaxation data presented herein, we have assumed that the relaxation properties of the ^{15}N spins are governed solely by the ^1H–^{15}N dipolar interaction and the CSA interaction. These two interactions are, however, not the only ones that can affect ^{15}N relaxation rates. For example, chemical-exchange processes can influence T_2 rates considerably (Kaplan & Fraenkel, 1980). These processes include exchange between several conformers occurring in specific regions of the protein, as will be discussed for the particular case of S. Nase in more detail below. In addition, the transverse ^{15}N relaxation rate is affected strongly by zero quantum magnetization exchange (spin flips) between the coupled NH proton and its proton neighbors. This latter contribution can be considered as scalar relaxation of the second kind (Bax et al., 1989b). Care must be exercised in the design of pulse schemes that measure transverse relaxation rates so that the effects of chemical exchange and zero quantum magnetization exchange are minimized. By use of the well-known Carr–Purcell–Meiboom–Gill (CPMG) pulse train (Carr & Purcell, 1954; Meiboom & Gill, 1958) during the transverse relaxation time T in the sequence of Figure 1b, these effects are substantially reduced. Only exchange processes occurring on a time scale faster than the time between the refocusing pulses in the CPMG sequence will remain. If, instead of the CPMG scheme, a 180° refocusing pulse had been employed in the middle of T (Nirmala & Wagner 1989), the contribution of scalar relaxation of the second kind to the measured ^{15}N line widths would be about 35% (Bax et al., 1989b), leading to a serious overestimate of the overall correlation time of the protein. The relative effect of scalar relaxation of the second kind on ^{13}C line widths is somewhat smaller since the magnitude of the ^{13}C–^1H dipolar interaction is larger than for ^{15}N–^1H pairs. For example, for a $^{13}C^{\alpha}H$ group in S. Nase the ^{13}C line width would include a contribution of ~15% from this relaxation process. Although small, errors of this magnitude are significant at the level of accuracy reported in this study.

Figure 3 shows six subspectra of ^1H–^{15}N correlation plots recorded at 600 MHz with the sequence of Figure 1a as a function of increasing values of T. As expected, the intensities of the cross-peaks decrease with increasing T. The resolution afforded by these experiments is significantly improved in comparison with the more commonly used heteronuclear multiple quantum correlation experiments (HMQC) (Bendall et al., 1983; Bax et al., 1983). More than 100 T_1 and T_2 values for ^{15}N spins have been extracted despite the traditional overlap problems associated with proteins the size of S. Nase.

Figure 4 shows ^{15}N decoupled one-dimensional ^1H spectra recorded with the sequence of Figure 1c with $t_1 = 0$ in the presence and absence of the ^1H–^{15}N NOE. The absence of signal intensity for nearly all residues in the difference spectrum (Figure 4c) indicates that the bulk of the residues in the protein are immobile and undergo reorientation with the whole molecule. The negative signals in the difference spectrum arise from a few residues with rapid large-amplitude internal motions. Unfortunately, the resolution is not sufficient in the one-dimensional spectra to assign any of the highly mobile resonances. The situation is improved dramatically in Figure 5 where positive (a) and negative (b) contour levels of a portion of the ^1H–^{15}N correlation spectrum recorded with the ^1H–^{15}N NOE are illustrated. The highly mobile resonances in Figure 5b are now easily assigned.

It should be emphasized that the interpretation of ^1H–^{15}N NOE data in a quantitative manner requires caution. As indicated by Smith et al. (1987), the long T_1 of water implies that if the recycle time is not sufficiently long, an NOE can be produced as a result of chemical exchange between the water and amide protons. This has the effect of artificially decreasing the measured NOEs. For example, we have measured the water T_1 to be 2.4 s in our sample. With a recycle time of 3 s approximately 20% of the water is saturated at the start of the experiment, giving rise to measured ^{15}N intensities for rapidly exchanging, highly mobile NH groups that are close to zero in spectra recorded without the ^1H–^{15}N NOE. For this reason, we have chosen not to interpret the NOEs in a quantitative sense, but to use them, qualitatively to determine those residues for which the effects of τ_e must be included in the interpretation of T_1 and T_2 data and to justify the neglect of these effects for the majority of the residues in S. Nase. The NOE data indicate that Leu-7, His-8, Ala-145, and Gly-148, as well as several residues that have only been identified by amino acid type, are all highly mobile. In particular, Ala-145 and Gly-148 have intense negative NOEs, suggesting significant contributions from rapid internal motions. In addition, the loop residues Gly-50, Val-51, and Glu-52 show NOEs lower (~0.6) than any of the other nonterminal residues.

Figure 6 shows bar graphs of ^{15}N T_1 and T_2 values recorded at 500 MHz for amide ^{15}N spins of S. Nase. As can be seen, effects of internal motion on T_1 and T_2 data are in some cases quite different for the same amino acid. This is a result of the fact that T_1 and T_2 values are sensitive to different motional frequencies. T_1 relaxation times provide information about motional properties with a frequency of approximately 10^8–10^{12} s^{-1}, while T_2 values, in addition to depending on motions occurring at these high frequencies, are also sensitive to dynamics on the micro- and millisecond time scale. By measuring both T_1 and T_2 relaxation times, it therefore is possible to obtain dynamic information over a large motional regime. Particularly striking are the T_2 results obtained for Glu-52 and Lys-53. The ^{15}N line widths of these two residues are about 2.5 times larger than the average ^{15}N line width obtained from the remainder of the assigned ^{15}N resonances. This is most likely the result of local conformational averaging

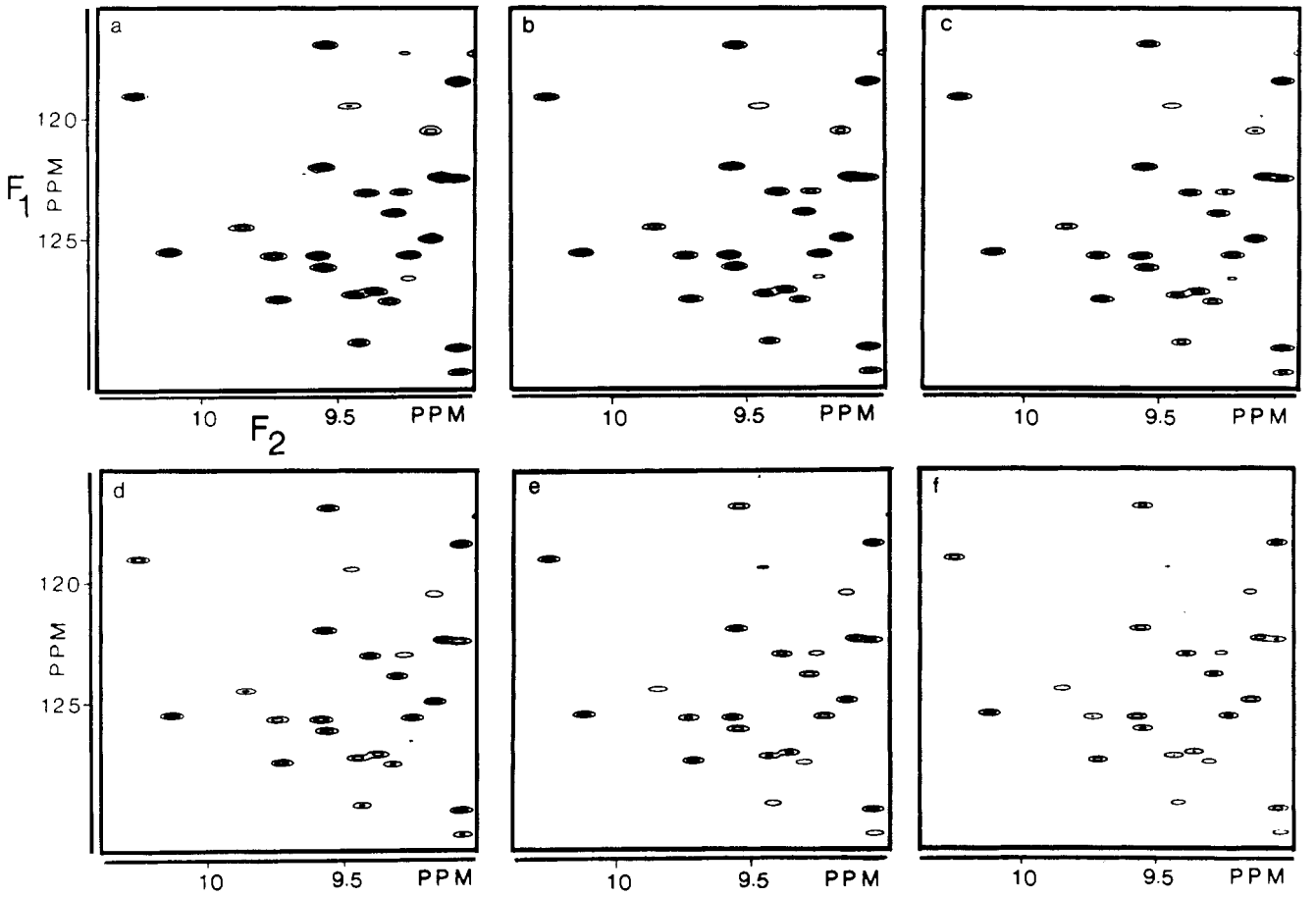

FIGURE 3: Contour plots of a small region of the ^1H–^{15}N correlation map of S. Nase recorded at 600 MHz with the sequence of Figure 1a. In (a–f) the values of T used are 50, 210, 370, 530, 690, and 850 ms. The peak intensities vary as $\exp(-T/T_1)$. The data sets were processed identically with Lorentzian to Gaussian weighting functions in t_2 and with a 70° shifted sine-bell function in t_1. Two zero fillings were employed in each dimension prior to Fourier transformation, giving final spectra with 1-Hz digital resolution in each dimension.

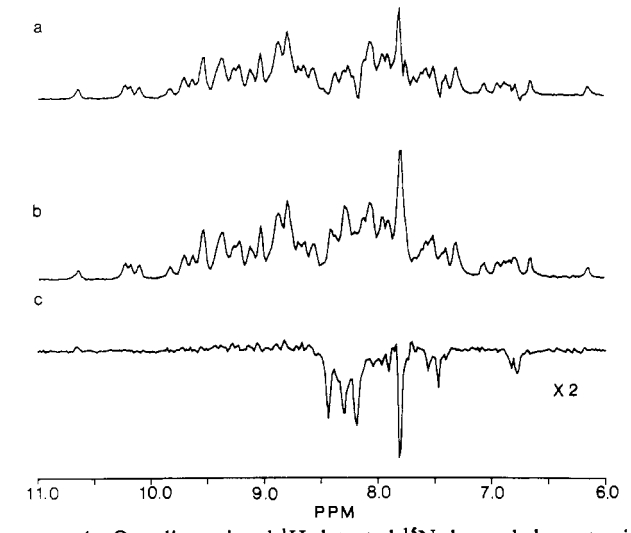

FIGURE 4: One-dimensional ^1H-detected ^{15}N-decoupled spectra in the presence (a) and absence (b) of the ^1H–^{15}N NOE. A total of 1024 scans were acquired per spectrum with a recycle time of 3 s (a) and 5 s (b). In (c) the difference spectrum [(a) − 0.8 × (b)] is shown.

at a rate comparable to the chemical shift differences of the various conformational forms. Amino acid Glu-52, for example, is at the end of a long disordered loop according to the X-ray structure (Loll & Lattman, 1989), and NMR studies of S. Nase (Torchia et al., 1989) have shown that the region from Pro-42 to Glu-57 is even more flexible and disordered in solution than in the crystal. Thr-22 and Val-23 also show significantly larger than average line widths, suggesting that in solution there is considerable flexibility of the β-bulge observed in the X-ray structure (Loll & Lattman, 1989). Since the line widths were measured with a CPMG sequence using a 1.2-ms delay between successive 180° pulses, a lower bound on the exchange rate between conformers is about 100 s^{-1}, assuming a two-site model.

As has been discussed previously, the relaxation data in this study have been anayzed by using a model which assumes isotropic motion. This assumption is quite reasonable for S. Nase. ^{13}C relaxation studies of Markley and co-workers (McCain et al., 1988) involving several glycine residues in S. Nase labeled in the $C^{\alpha}H$ position strongly suggested isotropic rotation of the protein. Moreover, correlation times, τ_m, calculated in the present study for each individual ^{15}N nucleus from the T_1/T_2 ratios are similar throughout the protein backbone, again suggesting isotropic motion. On the basis of the 1.65-Å X-ray structure of S. Nase (Loll & Lattman, 1989), the three principal components of the inertia tensor are calculated to be in the ratio of 1.00:1.31:1.39, again supporting the assertion that S. Nase behaves isotropically in solution. The average value of τ_m calculated in this study from T_1 and T_2 data, $\tau_m = 9.1 \pm 0.5$ ns, is in good agreement with values reported previously (McCain et al., 1988). This value was obtained by averaging all the values of τ_m calculated from measured T_1 and T_2 values at 500 and 600 MHz for 101 residues in S. Nase, using eq 8. Values of τ_m calculated for Thr-22, Val-23, Glu-52, and Lys-53 were excluded from this average since, as discussed above, a large contribution to the line width of these residues is due to conformational exchange broadening. In addition, the amino-terminal residues, Leu-7 and His-8, as well as the C-terminal residue, Gly-148, were excluded from the calculation since the assumption of negli-

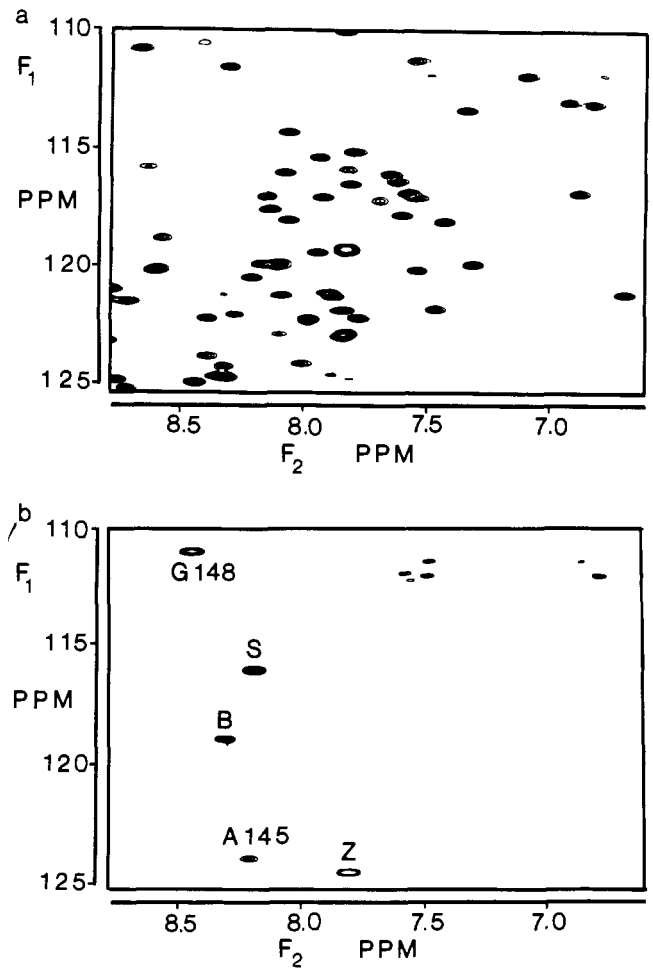

FIGURE 5: Positive (a) and negative (b) level contour plots of a small region of the ^1H–^{15}N NOE correlation map recorded with the scheme of Figure 1c. Both spectra are plotted with the same scale. Residues that are highly mobile give rise to the negative cross-peaks visible in (b).

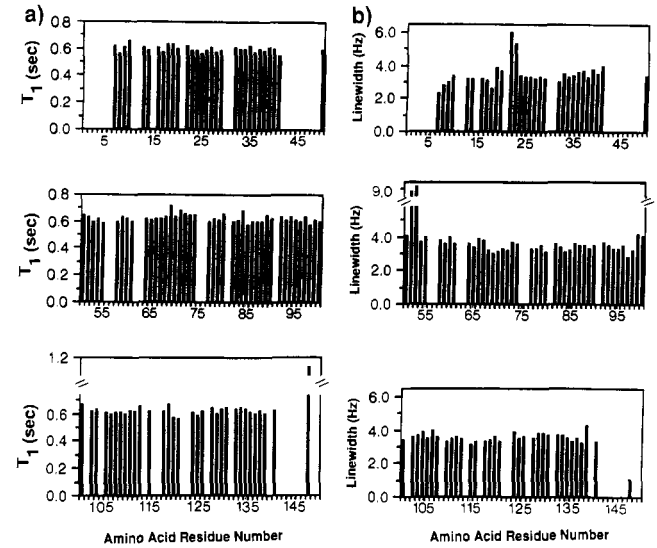

FIGURE 6: Bar graphs of ^{15}N T_1 (a) and line-width (b) values recorded at 500 MHz for backbone amide nitrogens of S. Nase. The line-width values were calculated from T_2 values obtained by use of a CPMG sequence [line width = $1/(\pi T_2)$].

gible τ_e values is clearly inappropriate for these highly mobile residues; i.e., the contributions to T_1 relaxation from rapid internal motions, characterized by τ_e, are no longer negligible.

Figure 7 shows a plot of S^2 vs amino acid residue number. The values of S^2 shown were obtained from averaging values

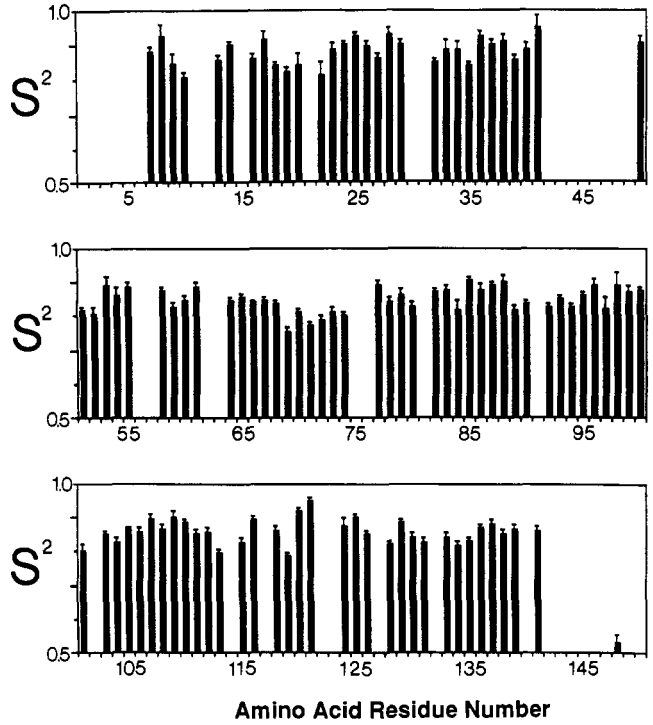

FIGURE 7: Values of S^2 vs amino acid for the backbone amide nitrogens of S. Nase. The values of S^2 shown are averages of the results obtained from data recorded at 500 and 600 MHz. The average rms error, σ_i, associated with each value of S^2 is indicated above each bar. The error, σ_i, is determined from the errors in S^2 calculated from data recorded at 500 MHz (σ_i^{500}) and data recorded at 600 MHz (σ_i^{600}) according to $\sigma_i = 0.5\{(\sigma_i^{500})^2 + (\sigma_i^{600})^2\}^{1/2}$. The values of σ_i^{500} and σ_i^{600} are easily calculated from the rms errors of the T_1 data recorded at 500 and 600 MHz, respectively (Shoemaker et al., 1962). An average S^2 of 0.86 is obtained for the whole protein (neglecting Leu-7, His-8, and Gly-148). In the cone model (Brainard & Szabo, 1981) this would correspond to motion within a semiangle of 18°. The values of S^2 calculated for Leu-7, His-8, and Gly-148 are overestimated since for these residues the contributions to T_1 from the rapid internal motions are no longer negligible. Using the full form of the spectral density function defined in eq 4, we obtain values of S^2 and τ_e of 0.54 and 0.21 ns (Leu-7), 0.71 and 0.12 ns (His-8), and 0.23 and 0.12 ns (Gly-148). With the cone model of Brainard and Szabo (1981) these values correspond to motion of the N–H bond vectors of residues 7, 8, and 148 in cones of semiangles 36°, 27°, and 53°.

calculated from eq 1 using the T_1 data recorded at 500 and 600 MHz and a τ_m value of 9.1 ns. In principle, S^2 values can also be calculated from eq 2 using T_2 data. Since T_2 rates are more likely to be influenced by relaxation mechanisms other than the dipolar and CSA mechanisms considered in eq 1 and 2, and because the exponential fitting of the T_2 decays gave relatively large rms errors (~5%), we prefer to use T_1 data exclusively in deriving the order parameters. Values of S^2 calculated from T_1s recorded at 500 and 600 MHz are in good agreement. This is evidenced by the fact that the rms difference of 0.026 between values of S^2 calculated from T_1 data recorded at 500 and 600 MHz is less than the sum of the average rms errors for values of S^2 obtained from data at 500 MHz (0.024) and 600 MHz (0.017). In contrast, the rms difference between values of S^2 calculated from T_1 data recorded at either 500 or 600 MHz and T_2 data is 0.085. This is well outside the error limits of the data and strongly suggests that contributions to T_2 from exchange processes are present in some cases.

As mentioned above, T_1 values were also recorded at 270 MHz. For molecules the size of S. Nase, for which $\omega_s\tau_m \sim 1.5$ at 270 MHz, ^{15}N relaxation times fall close to the minimum in the T_1 curve and hence do not provide as sensitive a measure of the overall molecular correlation time as do data

Table I: S^2 and Line Width vs Secondary Structure in S. Nase

secondary structure	S^2[a]	line width[a]	no. of residues averaged
α-helix	0.86 (0.03)	3.7 (0.2)	30
β-sheet	0.86 (0.04)	3.4 (0.6)	35
turns	0.86 (0.04)	3.7 (1.1)	27
loop (P42–E57)	0.86 (0.04)	5.5 (2.5)	6

[a] The values in parentheses correspond to the standard deviations.

recorded at higher fields. However, once the correlation time is known, in principle, accurate values of S^2 can be extracted that are relatively insensitive to errors in τ_m. Unfortunately, the uncertainty in the T_1 values recorded at 270 MHz is considerably greater than at 500 and 600 MHz due to the poorer quality of the correlation maps obtained. We have therefore not used these data in a quantitative manner.

The order parameters presented in Figure 7 were calculated by using an N–H bond distance of 1.02 Å obtained from neutron diffraction (Keiter, 1986). Since, in diffraction, ultrafast bond-stretching motions average the internuclear distances via $\langle r \rangle$, whereas for NMR relaxation the average is $\langle 1/r^3 \rangle$, an N–H value of 1.02 Å may not be completely accurate for the data considered here. It is important to bear in mind, therefore, that the absolute values of the order parameters reported in this study may have to be scaled appropriately. For example, an increase in the N–H bond length of 0.01 Å increases S^2 by ~6%. The relative values of the order parameters should be correct, however, under the assumption of equal N–H bond lengths throughout the protein.

The values of T_1 and S^2 presented in Figures 6 and 7 do not show any correlation with temperature factors (B factors) calculated from the X-ray analysis of S. Nase (Loll & Lattman, 1989). One of the reasons for the differences between the NMR and X-ray derived measurements of internal motions is that the B factors are sensitive to both fast and slow time-scale dynamics, whereas the values of S^2 are a function of rapid motions only. In this regard it is interesting to note that the largest temperature factors in S. Nase are found in the region of Gly-50 that, on the basis of the T_2 data, is close to that portion of the sequence appearing to be in conformational exchange. Loosli et al. (1985) and Nirmala and Wagner (1988) have also found little correlation between T_1 s of the α carbons and the B factors for cyclosporin A and BPTI, respectively.

A comparison of S^2 vs T_2 data indicates that there does not appear to be a correlation between high- and low-frequency fluctuations in S. Nase. For example, Thr-22, Val-23, Glu-52, and Lys-53 all have line widths that suggest localized conformational averaging on a millisecond time scale. The values of S^2 calculated for these four residues (0.81 ± 0.04, 0.89 ± 0.01, 0.81 ± 0.02, 0.89 ± 0.03), however, are not far from the average value of S^2 (0.86) calculated for the whole molecule. Consistent with these results, Wüthrich and co-workers have observed a lack of correlation between ^{13}C T_1 values and thermal stability in comparing two forms of BPTI (Richarz et al., 1980). Despite the fact that the two forms had differences in denaturation temperatures of over 20°, similar ^{13}C T_1 values were obtained for many of the measured resonances.

A particularly interesting question that can be addressed from the present study is how the order parameters change with different secondary structures in proteins. Table I shows the values of S^2 that have been obtained as a function of secondary structure determined from the X-ray results. As can be seen, to within the accuracy of the data, the values of the order parameter are completely independent of secondary structure.

A comparison of the ^{15}N line width with secondary structure in Table I indicates that the loop in the protein, which includes residues 42 through 56, appears to be more flexible on a millisecond time scale than the rest of the protein. The large increase in average line width of the loop region relative to other secondary structure motifs results from residues 52 and 53. It is interesting to note that Val-51 and Tyr-54 do not show an increase in ^{15}N line width despite the fact that the conformational heterogeneity in the loop region almost certainly includes these residues as well. However, the NH line width of Tyr-54 is particularly broad (Torchia et al., 1989). The apparent discrepancy between the ^{15}N and NH line widths of Tyr-54 may be explained by the fact that a significant chemical shift difference between the two exchanging conformers is required for exchange broadening to be manifest (Kaplan & Fraenkel, 1980). Another point of interest is that the data indicate a very narrow distribution of ^{15}N line widths for α-helices, slightly broader for β-sheets and still broader for turns and loops. It will be interesting to see whether these trends are also found for other proteins.

In summary, we have demonstrated the use of several new pulse schemes for the measurement of residue-specific backbone ^{15}N T_1, T_2, and NOE values. Unlike previous methods that have focused on the extraction of bulk relaxation times, or concentrated on the measurement of relaxation rates from a select number of labeled sites, the pulse schemes presented herein enable site-specific measurement of relaxation properties of macromolecules uniformly labeled with ^{13}C or ^{15}N. It is therefore possible to obtain dynamic information pertaining to each residue in proteins having molecular masses as large as 20 or 30 kDa. In the present study, accurate values of the order parameter have been extracted for 106 backbone amide ^{15}N nitrogens in S. Nase, providing a detailed measure of the extent of high-frequency motions in the protein backbone. This information will ultimately provide a more complete picture of proteins than has been previously accessible from static structures.

Added in Proof

The motional parameters reported for K84 should be assigned to K116. The parameters reported for K116 correspond to an unassigned lysine residue. We thank professor John Markley for sending us a preprint that caused us to reconsider the assignments of these two residues.

Acknowledgments

We thank Professor David Shortle for the plasmid encoding for the production of S. Nase, Dr. D. Baldisseri for providing the sample of S. Nase used in this study, and New Methods Research (Syracuse, NY) for making available a copy of their 2D NMR processing software.

Supplementary Material Available

Table containing T_1 values recorded at 270, 500, and 600 MHz as well as T_2 and NOE values recorded at 500 MHz, values of S^2 for each residue, and error values for each measurement (2 pages). Ordering information is given on any current masthead page.

Registry No. Staphylococcal nuclease, 9013-53-0.

References

Abragam, A, (1961) *The Principles of Nuclear Magnetism*, Clarendon Press, Oxford.

Allerhand, A., Doddrell, D., & Komoroski, R. (1971a) *J. Chem. Phys. 55*, 189.

Allerhand, A., Doddrell, D., Glushko, V., Cochran, D. W., Wenkert, E., Lawson, P. J. & Gurd, F. R. N. (1971b) *J. Am. Chem. Soc. 93*, 544.
Bax, A., Griffey, R. H., & Hawkins, B. L. (1983) *J. Magn. Reson. 55*, 301.
Bax, A., Sparks, S. W., & Torchia, D. A. (1989a) *Methods Enzymol. 176*, 134–150.
Bax, A., Ikura, M., Kay, L. E., Torchia, D. A., & Tschudin, R. (1989b) *J. Magn. Reson.* (in press).
Bendall, M. R., Pegg, D. T., & Doddrell, D. M. (1983) *J. Magn. Reson. 52*, 81.
Bodenhausen, G., & Ruben, D. J. (1980) *Chem. Phys. Lett. 69*, 185.
Bogusky, M. J., Schiksnis, R. A., Leo, G. C., & Opella, S. J. (1987) *J. Magn. Reson. 72*, 186.
Brainard, J. R., & Szabo, A. (1981) *Biochemistry 20*, 4618.
Brünger, A. T., Huber, R., & Karplus, M. (1987) *Biochemistry 26*, 5153.
Burum, D. P., & Ernst, R. R. (1980) *J. Magn. Reson. 39*, 163.
Carr, H. Y., & Purcell, E. M. (1954) *Phys. Rev. 94*, 630.
Dellwo, M. J., & Wand, A. J. (1989) *J. Am. Chem. Soc. 111*, 4571.
Fuson, M., & Prestegard, J. H. (1983) *Biochemistry 22*, 1311.
Glushko, V., Lawson, P. J., & Gurd, F. R. N. (1972) *J. Biol. Chem. 247*, 3176.
Gust, D., Moon, R. B., & Roberts, J. D. (1975) *Proc. Natl. Acad. Sci. U.S.A. 72*, 4696.
Hawkes, G. E., Randall, E. W., & Bradley, C. H. (1975) *Nature (London) 257*, 767.
Henry, G. D., Weiner, J. H., & Sykes, B. D. (1986) *Biochemistry 25*, 590.
Hibler, D. W., Stolowich, N. J., Reynolds, M. A., Gerlt, J. A., Wilde, J. A., & Bolton, P. H. (1987) *Biochemistry 26*, 6278.
Hiyama, Y., Niu, C., Silverton, J. V., Bavoso, A., & Torchia, D. A. (1988) *J. Am. Chem. Soc. 110*, 2378.
Kaplan, J. I., & Fraenkel, G. (1980) *NMR of Chemically Exchanging Systems*, Academic Press, New York.
Kay, L. E., Jue, T., Bangerter, B., & Demou, P. C. (1987) *J. Magn. Reson. 73*, 558.
Kay, L. E., Marion, D., & Bax, A. (1989) *J. Magn. Reson. 84*, 72.
Keiter, E. A. (1986) Ph.D. Thesis, University of Illinois.
Kuhlmann, K. F., Grant, D. M., & Harris, R. K. (1970) *J. Chem. Phys, 52*, 3439.
LeMaster, D., Kay, L. E., Brünger, A. T., & Prestegard, J. H. (1988) *FEBS Lett. 236*, 71.
Levy, R. M., Karplus, M., & McCammon, J. A. (1981) *J. Am. Chem. Soc. 103*, 994.
Lipari, G., & Szabo, A. (1982a) *J. Am. Chem. Soc. 104*, 4546.
Lipari, G., & Szabo, A. (1982b) *J. Am. Chem. Soc. 104*, 4559.
Llinas, M., & Wüthrich, K. (1978) *Biochim. Biophys. Acta 532*, 29.
Loll, P. J., & Lattman, E. E. (1989) *Proteins: Struct. Funct., Genet.* (submitted for publication).
London, R. E. (1980) *Magn. Reson. Biol. 1*, 1.
Loosli, H. R., Kessler, H., Oschkinat, H., Weber, H. P., Petcher, T., & Widmer, A. (1985) *Helv. Chim. Acta 68*, 682.
Marion, D., & Wüthrich, K. (1983) *Biochem. Biophys. Res. Commun. 113*, 967.
Markley, J. L., Horsley, W. J., & Klein, M. P. (1971) *J. Chem. Phys. 55*, 3604.
McCain, D. C., & Markley, J. L. (1986) *J. Am. Chem. Soc. 108*, 4259.
McCain, D. C., Ulrich, E. L., & Markley, J. L. (1988) *J. Magn. Reson. 80*, 296.
Meiboom, S., & Gill, D. (1958) *Rev. Sci. Instrum. 29*, 688.
Morris, G. A., & Freeman, R. (1979) *J. Am. Chem. Soc. 101*, 760.
Nirmala, N. R., & Wagner, G. (1988) *J. Am. Chem. Soc. 110*, 7557.
Nirmala, N. R., & Wagner, G. (1989) *J. Magn. Reson. 82*, 659.
Norton, R. E., Clouse, A. O., Addleman, R., & Allerhand, A. (1977) *J. Am. Chem. Soc. 99*, 79.
Olejniczak, E. T., Dobson, C. M., Karplus, M., & Levy, R. M. (1984) *J. Am. Chem. Soc. 106*, 1923.
Richarz, R., Nagayama, K., & Wüthrich, K. (1980) *Biochemistry 19*, 5189.
Schiksnis, R. A., Bogusky, M. J., Tsang, P., & Opella, S. J. (1987) *Biochemistry 26*, 1373.
Shoemaker, D. P., Garland, C. W., Steinfeld, J. I., & Nibler, J. W. (1962) *Experiments in Physical Chemistry*, 4th ed., McGraw-Hill, New York.
Sklenár, V., Torchia, D., & Bax, A. (1987) *J. Magn. Reson. 73*, 375.
Smith, G. M., Yu, P. L., & Domingues, D. J. (1987) *Biochemistry 26*, 2202.
States, D. J., Haberkorn, R., & Ruben, D. J. (1982) *J. Magn. Reson. 48*, 268.
Torchia, D. A., Sparks, S. W., & Bax, A. (1989) *Biochemistry 28*, 5509.
Werbelow, L. (1987) *J. Chem. Soc., Faraday Trans. 2 83*, 897.